Supplementary Material

Branching fraction measurements

The comparison of the $B^+ \to K^+\mu^+\mu^-$ branching fraction from Ref. [1] to the $B^+ \to K^+e^+e^-$ branching fraction resulting from the measurement of R_K presented in this paper is shown in Fig. S1. The uncertainty stemming from the branching fractions of the corresponding normalisation channels is folded into the total uncertainty of each measurement.

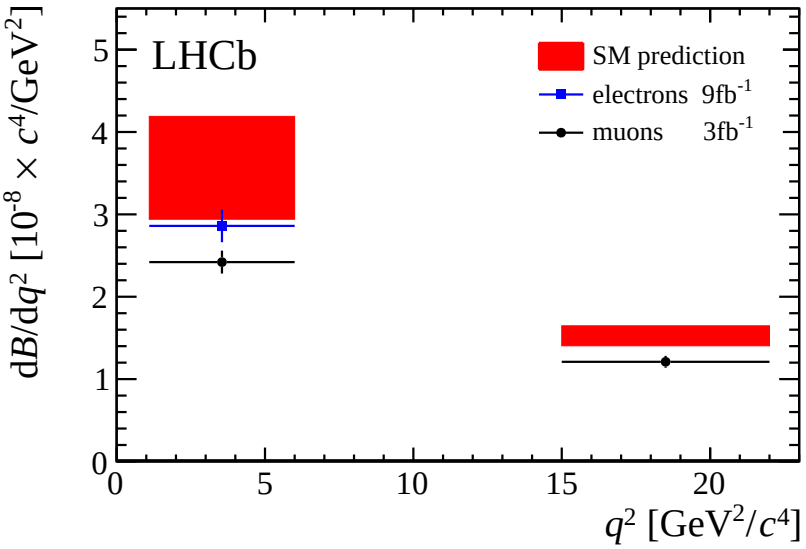

Figure S1: Branching fractions of (blue) $B^+ \to K^+e^+e^-$ from this paper and (black) $B^+ \to K^+\mu^+\mu^-$ from Ref. [1] including the q^2 bin $15.0 < q^2 < 22.0\,\text{GeV}^2/c^4$. The SM predictions (red area) from Refs. [2, 3] are also shown.

Fits to the $B^+ \to \psi(2S)K^+$ resonant mode

The fits to the resonant $B^+ \to \psi(2S)K^+$ decay mode in different data-taking periods and trigger categories are shown in Fig. S2. The strong correlation between the combinatorial background and the partially reconstructed decays from higher charmonium resonances causes the variation of the fitted mass shapes across data-taking periods and trigger categories. However, this has a negligible effect on the signal yield extraction as the sum of the two contributions is constant across data-taking periods and trigger categories.

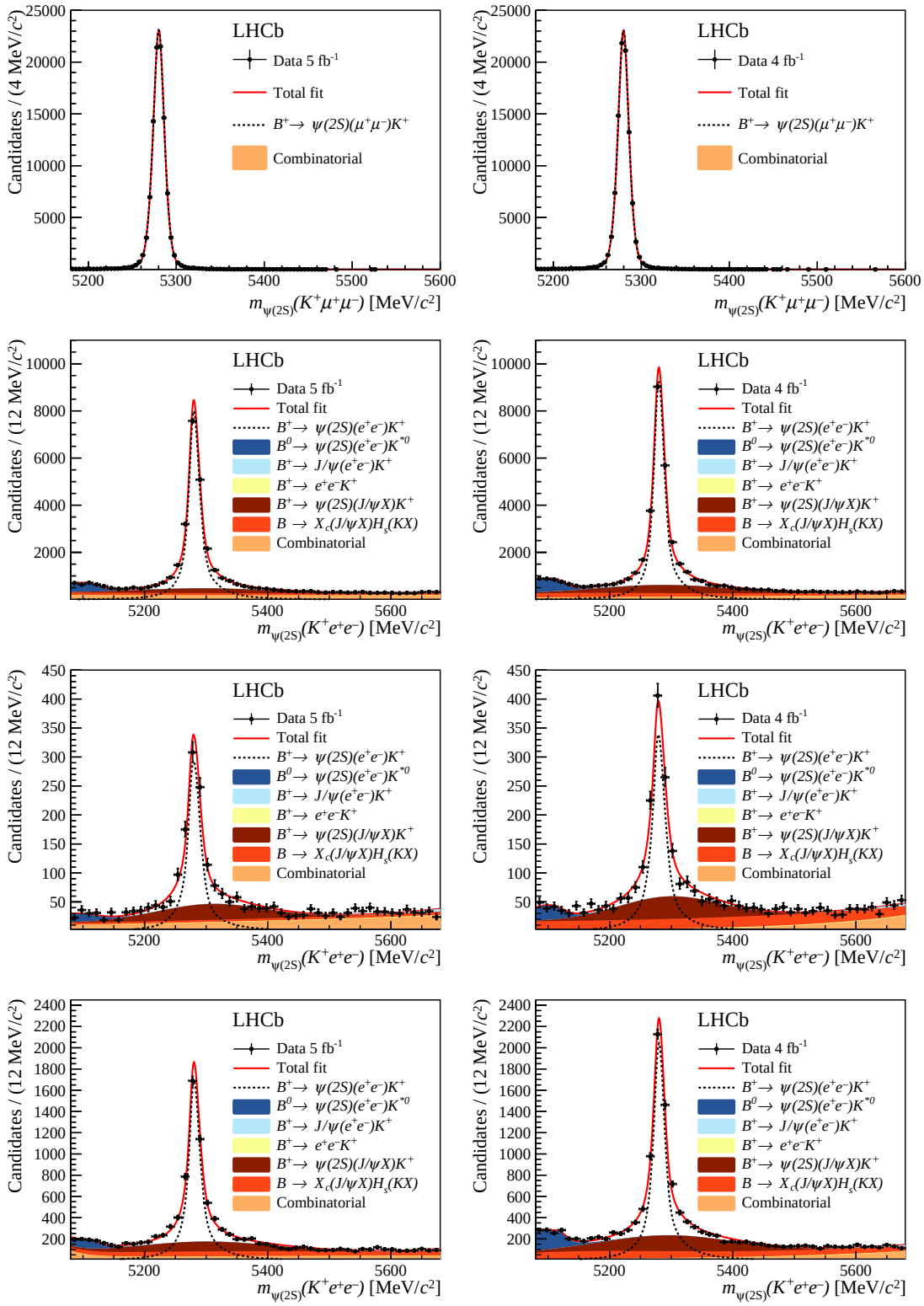

Figure S2: Candidate invariant mass distributions. Distribution of the invariant mass $m_{\psi(2S)}(K^+\ell^+\ell^-)$ for $B^+ \to \psi(2S)K^+$ resonant candidates in the (left) sample previously analysed [4] and (right) the new data sample. The top row shows the fit to the muon modes, the combinatorial component is included in the fit but is too small to be seen. The subsequent rows show the fits to the electron modes triggered by (second row) one of the electrons, (third row) the kaon and (last row) by other particles in the event. The fit projections are superimposed.

Effect of q^2 migration

Due to the finite resolution in q^2, signal candidates with a true q^2 (q^2_{true}) outside the interval of interest can be reconstructed with $1.1 < q^2 < 6.0$ GeV$^2/c^4$. The contribution from $B^+ \to K^+e^+e^-$ candidates that undergo this q^2 migration is show in Fig. S3 for simulation and Fig. S4 for data.

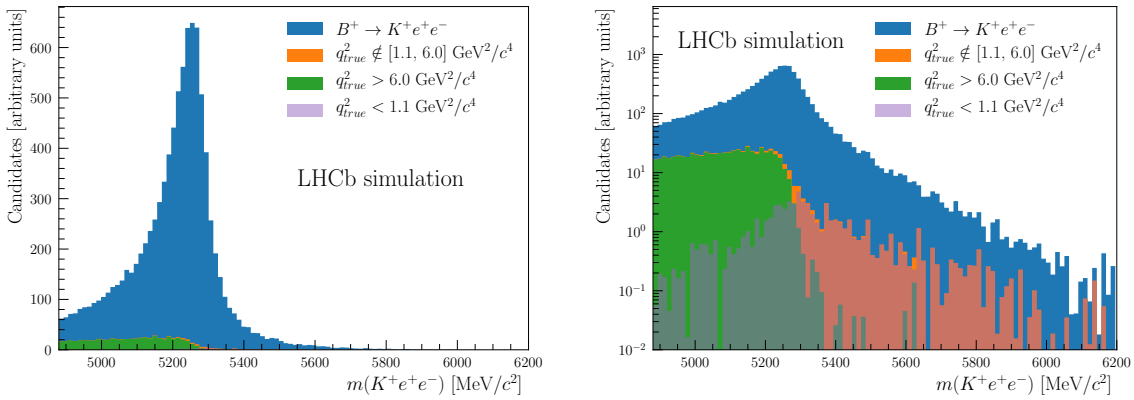

Figure S3: Distribution of $m(K^+e^+e^-)$ in simulated $B^+ \to K^+e^+e^-$ decays. The orange shaded area corresponds to $B^+ \to K^+e^+e^-$ candidates with true q^2 outside the interval of interest. The green and purple components correspond to candidates with $q^2_{\text{true}} > 6.0$ GeV$^2/c^4$ and $q^2_{\text{true}} < 1.1$ GeV$^2/c^4$, respectively. (Left) linear and (right) logarithmic scales are shown.

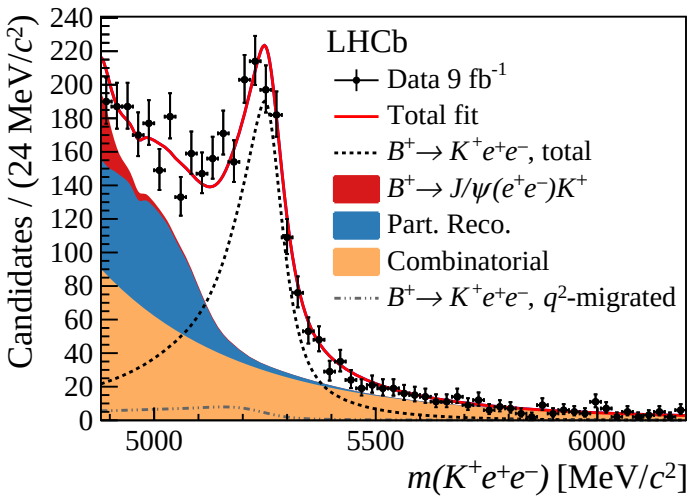

Figure S4: Distribution of the invariant mass $m(K^+e^+e^-)$ for $B^+ \to K^+e^+e^-$ candidates. The fit projection is superimposed, with a black dotted line describing the signal contribution and solid areas representing each of the background components described in the text and listed in the legend. For illustration, the expected distribution of signal candidates with $q^2_{\text{true}} < 1.1$ GeV$^2/c^4$ or $q^2_{\text{true}} > 6.0$ GeV$^2/c^4$ is shown as a grey dashed and dotted line.

Overview of R_K measurements

An overview of available measurements of R_K in different q^2 regions is given in Fig S5. Previous LHCb measurements are also included for comparison in Fig S6 and Fig S7.

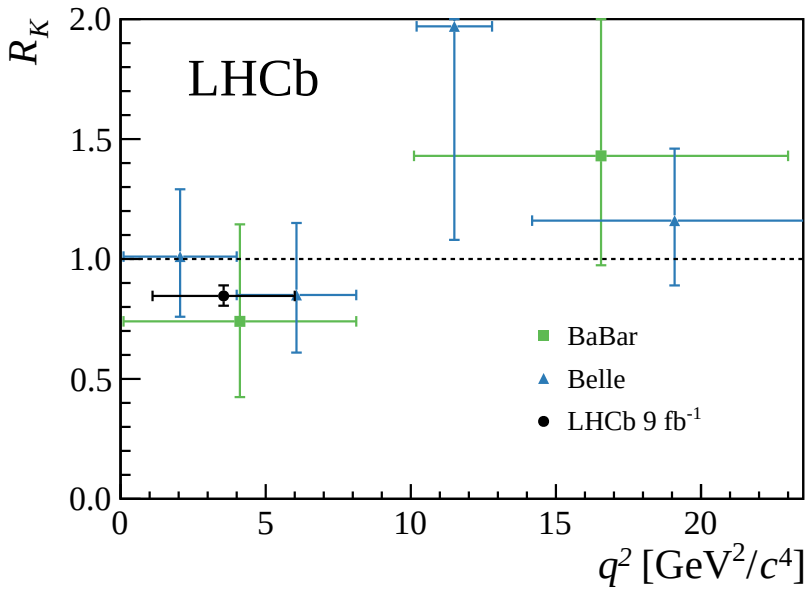

Figure S5: Comparison between R_K measurements. The measurements by the BaBar [5] and Belle [6] collaborations combine $B^+ \to K^+\ell^+\ell^-$ and $B^0 \to K^0_S\ell^+\ell^-$ decays.

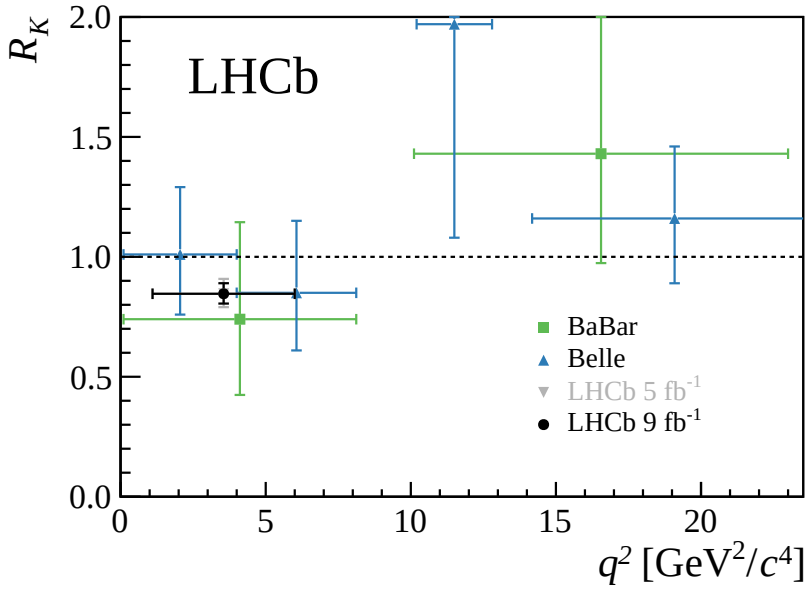

Figure S6: Comparison between R_K measurements. The measurements by the BaBar [5] and Belle [6] collaborations combine $B^+ \to K^+\ell^+\ell^-$ and $B^0 \to K^0_S\ell^+\ell^-$ decays. The previous LHCb measurement [4], superseded by the present result, is also shown.

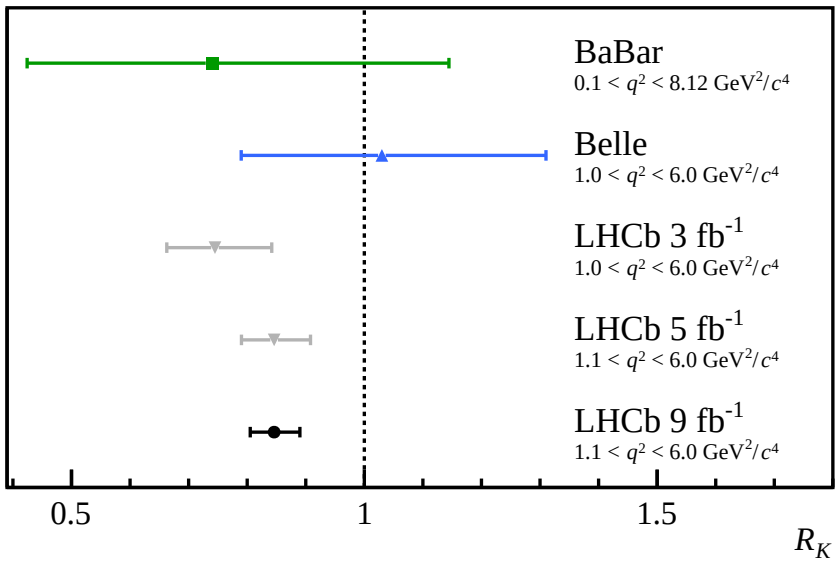

Figure S7: Comparison between R_K measurements. The measurements by the BaBar [5] and Belle [6] collaborations combine $B^+ \to K^+\ell^+\ell^-$ and $B^0 \to K^0_S\ell^+\ell^-$ decays. The previous LHCb measurements [4] and [7], superseded by the present result, are also shown.

References

[1] LHCb collaboration, R. Aaij *et al.*, *Differential branching fractions and isospin asymmetries of $B \to K^{(*)}\mu^+\mu^-$ decays*, JHEP **06** (2014) 133, arXiv:1403.8044.

[2] J. A. Bailey *et al.*, *$B \to K l^+ l^-$ decay form factors from three-flavor lattice QCD*, Phys. Rev. **D93** (2016) 025026, arXiv:1509.06235.

[3] D. Du *et al.*, *Phenomenology of semileptonic B-meson decays with form factors from lattice QCD*, Phys. Rev. **D93** (2016) 034005, arXiv:1510.02349.

[4] LHCb collaboration, R. Aaij *et al.*, *Search for lepton-universality violation in $B^+ \to K^+\ell^+\ell^-$ decays*, Phys. Rev. Lett. **122** (2019) 191801, arXiv:1903.09252.

[5] BaBar collaboration, J. P. Lees *et al.*, *Measurement of branching fractions and rate asymmetries in the rare decays $B \to K^{(*)}\ell^+\ell^-$*, Phys. Rev. **D86** (2012) 032012.

[6] Belle collaboration, S. Choudhury *et al.*, *Test of lepton flavor universality and search for lepton flavor violation in $B \to K\ell\ell$ decays*, JHEP **03** (2021) 105, arXiv:1908.01848.

[7] LHCb collaboration, R. Aaij *et al.*, *Test of lepton universality using $B^+ \to K^+\ell^+\ell^-$ decays*, Phys. Rev. Lett. **113** (2014) 151601, arXiv:1406.6482.